Lithospheric Stress and Strain Models: Constraints from a Global Dataset of Surface Faults. L. L. Dimitrova[1], W. E. Holt[1], A. J. Haines[2] and R. A. Schultz[3], [1]Department of Geosciences, SUNY at Stony Brook, Stony Brook, NY 11794 (Lada.Dimitrova@stonybrook.edu, William.Holt@stonybrook.edu), [2]Department of Earth Sciences, University of Cambridge, UK (ajh50@cam.ac.uk), [3]Department Department of Geological Sciences and Engineering, University of Nevada, Reno, NV (schultz@mines.unr.edu).

Introduction: A planet's evolution is recorded, in part, in the surficial expression of the tectonic features observed today. Theoretical models of deformation mechanisms can be compared to the surficial expression of the tectonic features observed today and interpreted in terms of major tectonic events, thus allowing us insights into the internal structure and processes on Mars. For this study we focus on the expected style, orientation, and magnitudes of stress and associated strain.

Global geologic maps as early as 1986 show that the normal faults associated with the formation of Tharsis extend over almost half of Mars [1] and are thus a dominant part in the global tectonic evolution of Mars. Historically, combinations of mechanisms -- lithospheric uplift, isostasy, and flexure -- have been used to explain the faulting [2], while more recently [3] argued that the membrane and flexure model of [4] is sufficient. Membrane and flexure models produce no deviatoric extension in the area of loading, and as pointed out by [4] the faulting extending from northern Claritas Fossae north and north-east through Tantalus and Alba Fossae is not well described by such models.

An alternative model ([5]), based on stresses associated with gravitational potential energy (GPE) differences, has been shown to fit (~70%) of the normal faults in Tharsis, as mapped by [6]. This fit implies that possibly the normal faults in and around Tharsis formed early in the Martian history when elastic thicknesses as well as membrane and flexural stresses were small, and viscous rather than elastic processes dominated. Alternatively, the combined stress from other sources (e.g. flexure, global contraction, etc.), which may have dominated the GPE stresses, must agree with the stresses associated with GPE differences.

The majority of the misfit in [5] is restricted to the region north and northeast of Alba Patera and can be explained with modest crustal density variations ($\leq$170kg·m^{-3}), and even smaller variations in both the mantle and crustal densities [7]. In addition, membrane stresses can also explain the misfit, but are ill-constrained by the fault data.

The studies of [5,7] were biased towards the normal faults in the western hemisphere due the available data set. Recent orbital exploration has led to the creation of expanded fault data sets [8,9]. We now extend these studies to use the fault data from [8].

Methodology: As in [5], we perform a Kostrov moment tensor summation to estimate the total strain tensor associated with the fault segments of [8]. We have assumed a uniform amount of slip for each fault as a first approximation. We use an objective inner product measure [5] to estimate the misfit of the GPE associated model of stress to the calculated strain.

We perform inversions minimizing the surface integral of the misfit for additional stresses due to GPE variations or membrane displacements. To do this we use a forward thin-sheet model [9] to calculate the Green's function responses to forcing terms of spherical harmonics degree and order 9. We invert for the coefficients for these Green's functions responses such that the resultant stress field, when added to the GPE stress field, minimizes the surface integral of the misfit. We sum the spherical harmonics weighted by these coefficient to calculate the corresponding membrane displacements or GPE changes. The GPE variations are interpreted in end-member cases as density variations and Moho depth variations.

Results: *Fault strain.* The normal and reverse faults are shown in Fig 1. Note that the normal faults are located predominantly in the western hemisphere while the reverse faults have a more global distribution.

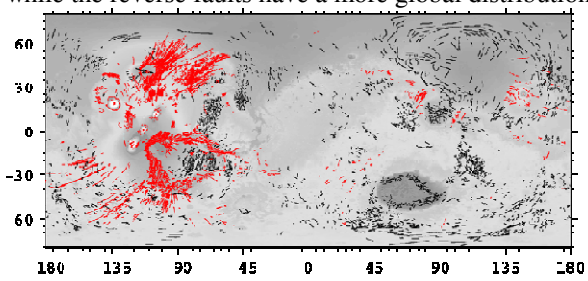

Figure 1 Normal (in red) and reverse (in black) faults from [8].

The strain from the Kostrov calculation for the extensional and compressional faults is shown in Fig 2. Almost all normal faults are located in high topography areas, with the exception of faults along the dichotomy boundary in the eastern hemisphere and north/northeast of Alba Patera. Since the GPE associated stresses tend to be deviatorically extensional in areas of high topography, the fit to the normal faults is high (Fig 3A). The abundance of reverse faults in the high topography areas of the southern hemisphere leads to a much poorer fit of the GPE associated stresses to the reverse faults (Fig 3B).

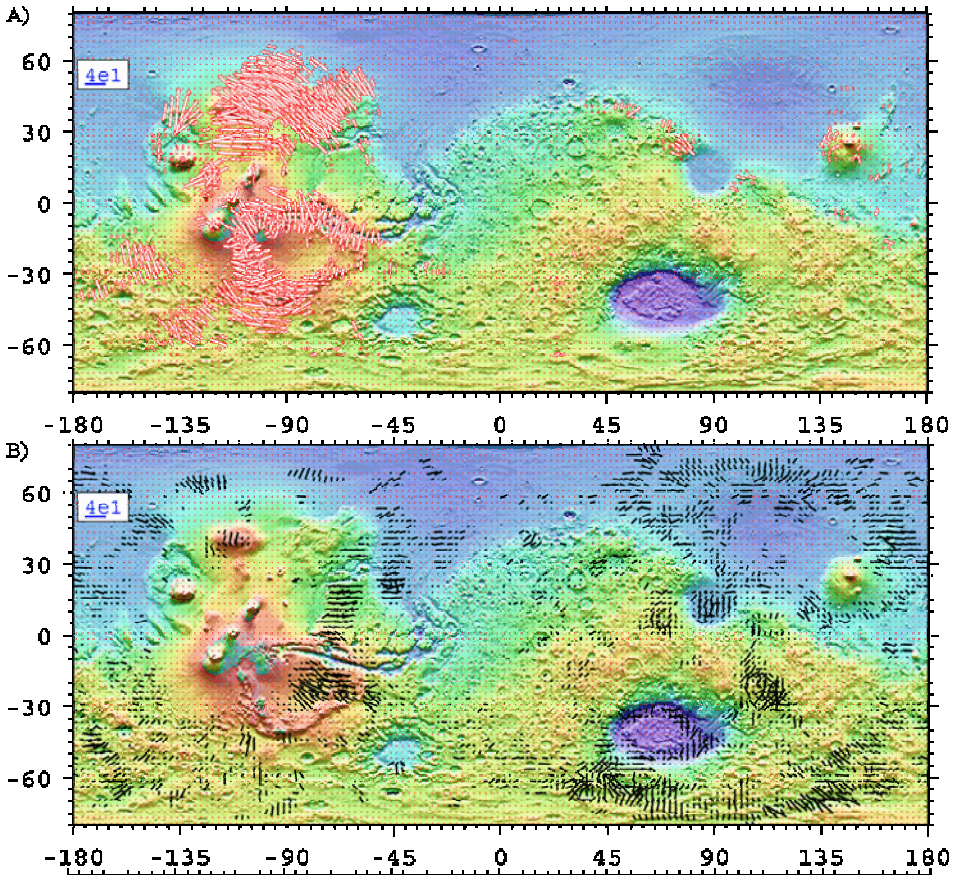

Figure 2. Deviatoric strain from Kostrov summation associated with A) the normal faults and B) the reverse faults of [8]. Red open arrows represent deviatoric extension, while black filled-in arrows represent deviatoric compression. Note that we have assumed a uniform amount of slip for each fault as a first approximation. Consequently, the magnitude of the calculated strain does not reflect the real absolute strain. Accordingly, our misfit measure depends only on the relative magnitude and orientation of the principal strains.

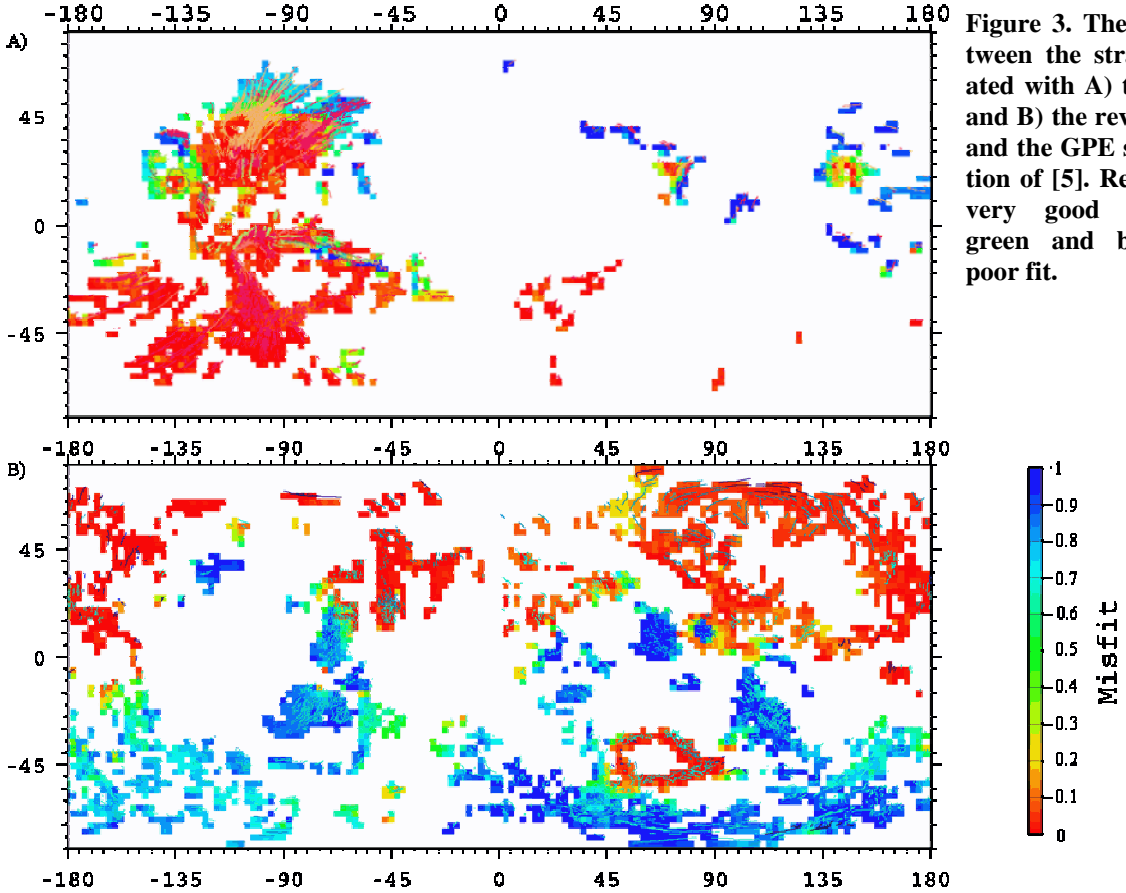

Figure 3. The misfit between the strain associated with A) the normal and B) the reverse faults and the GPE stress solution of [5]. Red means a very good fit, while green and blue mean poor fit.

For each type of fault, we perform inversions minimizing the surface integral of the misfit for additional stresses due to GPE variations only or membrane displacements only based on Green's function responses to forcing terms of spherical harmonics degree and order 9. The resulting surface integral of the residual misfit for each degree and order, as well as the number of coefficients solved for, is shown in Table 1.

Table 1. Surface integral of the residual misfit by spherical degree and order cut-off, inversion and type of fault for each inversion.

spherical degree and order cut-off/ number of coefficients	surface integral of the residual misfit	
	normal faults (539 base)	reverse faults (1806 base)
Inversion for additional GPE only		
2/5	445	1479
3/12	369	1305
4/21	295	975
5/32	244	711
6/45	216	670
7/60	188	610
8/77	172	576
9/96	158	543
Inversion for membrane displacement only		
2/5	508	1741
3/12	457	1676
4/21	399	1565
5/32	370	1430
6/45	348	1368
7/60	326	1290
8/77	302	1187
9/96	261	1120

Inversion for additional GPE. The additional GPE, as well as the fit to the faults for our inversion of degree and order up to 5, is shown in Fig 4. For the normal faults, the improvement is north/north-east of Alba Patera and north/northeast portion of Arabia Terra, while minor improvement is seen in the vicinity of Elysium Mons. The additional GPE is characterized by three highs – a high north/north-east of Alba Patera in the western hemisphere, and highs around Hellas and Utopia Planitae in the eastern hemisphere. The GPE high around Valles Marineris is a result of two factors (1) the width of Valles Marineris is larger than our grid size, and (2) while the GPE stress model of [5] around Valles Marineris is consistent with its formation, once the feature is created, the low topography will lead to compressional GPE stresses inside the rift. The additional GPE can be achieved with variations in crustal density alone of $\pm 43 kg \cdot m^{-3}$, mantle density alone of $\pm 272 kg \cdot m^{-3}$, or both crustal and mantle density of $\pm 25 kg \cdot m^{-3}$.

For the reverse faults, significant improvement is seen for the "classical" wrinkle ridges in Solis and Lunae Plana, while some improvement is seen in Sirenum Terra and in the highlands surrounding Hellas Planitia. The additional GPE is characterized by two highs in the eastern hemisphere at Hellas and Utopia Planitia, consistent with results from the normal faults. In the western hemisphere, however, there is little correlation between the GPE from the normal and reverse faults, and furthermore, the low GPE at Alba Patera is opposite from the high GPE required by the normal faults. The additional GPE can be achieved with variations in crustal density alone of $\pm 57 kg \cdot m^{-3}$, mantle density alone of $\pm 207 kg \cdot m^{-3}$, or both crustal and mantle density of $\pm 34 kg \cdot m^{-3}$.

Inversion for additional membrane displacement. For a given spherical degree and order cut-off, the stresses associated with membrane displacement fit the normal faults slightly worse than the stresses with additional GPE (Table 1); the additional membrane misfit is north/north-east of Alba Patera. Comparing the membrane model with spherical degree and order 5 cut-off with the additional GPE model of the same cut-off, there is a correlation between areas of upward membrane displacement in the areas of high additional GPE at Hellas and Utopia Planitae in the eastern hemisphere, and north/north-east of Alba Patera. The additional membrane displacements are within ± 472m.

The membrane displacement model fails to improve the fit to the reverse faults even for spherical degree and order 9 cut-off. The major area of improvement is to the wrinkle ridges in Lunae Planum, and to a lesser degree to reverse faults just north/north-east and south/south-west of Hellas Planitia.

Summary: The normal faults mapped to-date are clustered in the western hemisphere around Tharsis, and hence, provide a poor constraint on processes elsewhere. On the other hand, the reverse faults are much more uniformly distributed; in particular, reverse faults in high topography areas remain difficult to fit with global models of lithospheric deformation. Stresses associated with GPE provide the best fit to the faults, while membrane stresses up to degree and order 9 fail to fit the reverse faults. Inversion results for the western hemisphere are either decorrelated or negatively correlated; however, the inversions for the eastern hemisphere require a combination of removal of material and subsidence after the fault formation.

References: [1] Scott & Tanaka (1986) *USGS Map I-1802-A*. [2] Banerdt et al. (1992) *Mars*, 249-297. [3] Phillips et al. (1999) *Science* **292**, 2587-2591. [4] Banerdt et al. (2000) *LPS XXXI,* Abstract #2038. [5] Dimitrova et al. (2006) *GRL* **33**, L08202. [6] Anderson et al. (2001) *JGR* **106**, 20563-20585. [7] Dimitrova et al. (in preparation). [8] Knapmeyer et al. (2006) *JGR* **111**, E11006. [9] Flesch et al. (2001) *JGR* **106**, 16435-16460.

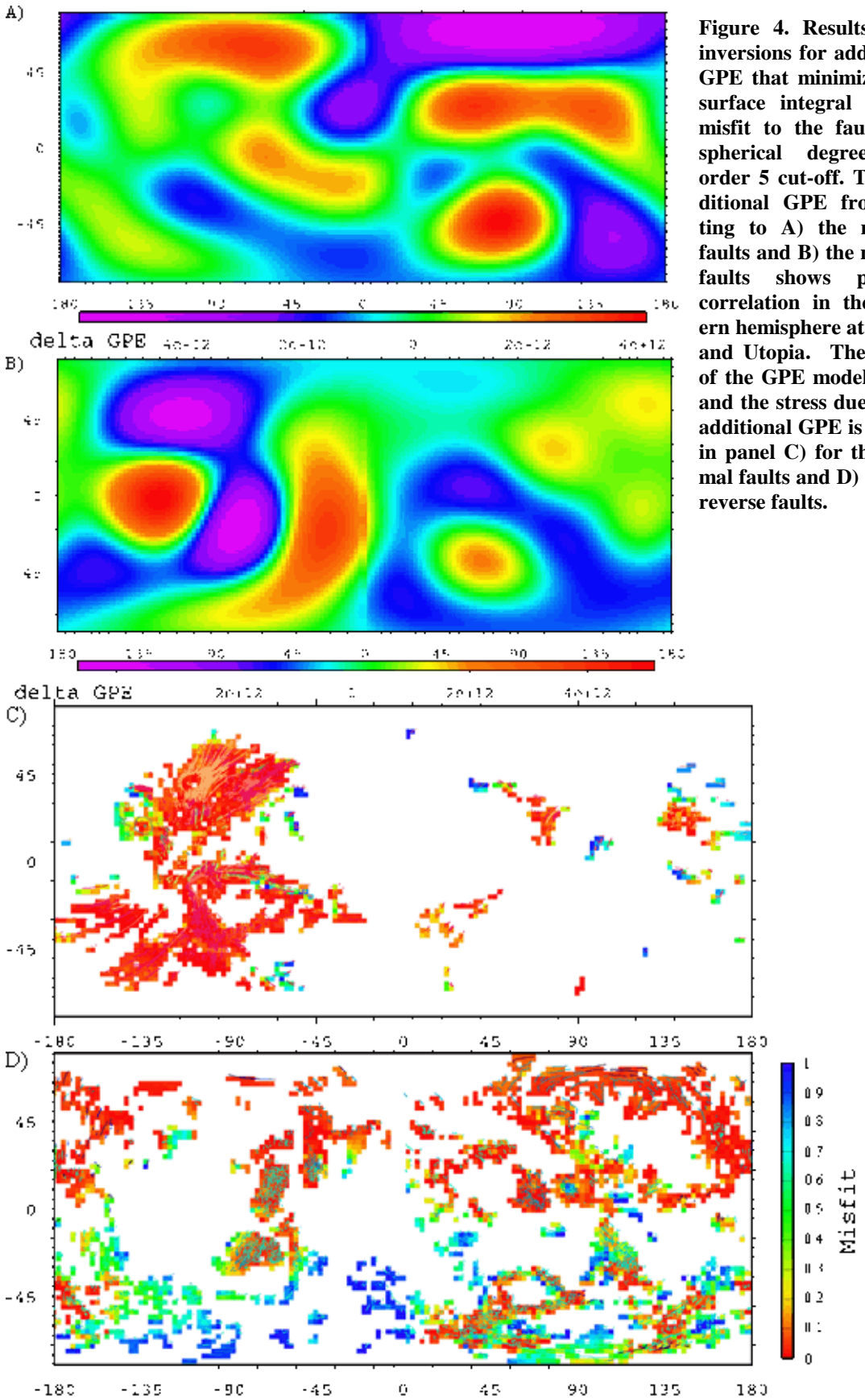

Figure 4. Results from inversions for additional GPE that minimizes the surface integral of the misfit to the faults for spherical degree and order 5 cut-off. The additional GPE from fitting to A) the normal faults and B) the reverse faults shows positive correlation in the eastern hemisphere at Hellas and Utopia. The misfit of the GPE model of [5] and the stress due to the additional GPE is shown in panel C) for the normal faults and D) for the reverse faults.